Regulation of the HIF-1α Level Is Essential for Hematopoietic Stem Cells

Keiyo Takubo,[1,*] Nobuhito Goda,[3,6] Wakako Yamada,[1] Hirono Iriuchishima,[1] Eiji Ikeda,[4] Yoshiaki Kubota,[1] Haruko Shima,[1] Randall S. Johnson,[5] Atsushi Hirao,[6,7] Makoto Suematsu,[2] and Toshio Suda[1,*]
[1]Department of Cell Differentiation, The Sakaguchi Laboratory of Developmental Biology, Keio University School of Medicine, 35 Shinano-machi, Shinjuku-ku, Tokyo 160-8582, Japan
[2]Department of Biochemistry, Keio University School of Medicine and JST-ERATO, Suematsu Gas Biology Project, 35 Shinano-machi, Shinjuku-ku, Tokyo 160-8582, Japan
[3]Department of Life Science and Medical Bio-Science, School of Advanced Science and Engineering, Waseda University, 2-2 Wakamatsu-cho, Shinjuku-ku, Tokyo, 162-8480, Japan
[4]Department of Pathology, Yamaguchi University Graduate School of Medicine, 1-1-1 Minami-Kogushi, Ube, Yamaguchi, 755-8505, Japan
[5]Molecular Biology Section, Division of Biological Sciences, University of California, San Diego, 9500 Gilman Drive, La Jolla, CA 92093, USA
[6]Core Research for Evolutional Science and Technology, Japan Science and Technology Agency, Chiyoda-ku, Tokyo 102-0075, Japan
[7]Division of Molecular Genetics, Cancer Research Institute, Kanazawa University, Kakuma-machi, Kanazawa 920-1192, Japan
*Correspondence: keiyot@gmail.com (K.T.), sudato@sc.itc.keio.ac.jp (T.S.)
DOI 10.1016/j.stem.2010.06.020

SUMMARY

Hematopoietic stem cells (HSCs) are sustained in a specific microenvironment known as the stem cell niche. Mammalian HSCs are kept quiescent in the endosteal niche, a hypoxic zone of the bone marrow (BM). In this study, we show that normal HSCs maintain intracellular hypoxia and stabilize hypoxia-inducible factor-1α (HIF-1α) protein. In HIF-1α-deficient mice, the HSCs lost their cell cycle quiescence and HSC numbers decreased during various stress settings including bone marrow transplantation, myelosuppression, or aging, in a p16^{Ink4a}/p19^{Arf}-dependent manner. Overstabilization of HIF-1α by biallelic loss of an E3 ubiquitin ligase for HIF-1α (VHL) induced cell cycle quiescence in HSCs and their progenitors but resulted in an impairment in transplantation capacity. In contrast, monoallelic loss of VHL induced cell cycle quiescence and improved BM engraftment during bone marrow transplantation. These data indicate that HSCs maintain cell cycle quiescence through the precise regulation of HIF-1α levels.

INTRODUCTION

Stem cells localize to specific sites, or "niches," in the tissues, where they are preferentially maintained by various environmental factors (Scadden, 2006; Morrison and Spradling, 2008; Li and Xie, 2005). Mammalian bone marrow (BM) has been suggested to be relatively hypoxic compared to other tissues, and primitive hematopoietic cells including hematopoietic stem cells (HSCs) are thought to be localized in the most hypoxic microenvironment of the BM (Cipolleschi et al., 1993; Levesque et al., 2007; Parmar et al., 2007; Kubota et al., 2008). The hypoxic ex vivo culture of BM cells or primitive hematopoietic progenitors results in maintenance of the primitive phenotype (Danet et al., 2003) and cell cycle quiescence (Hermitte et al., 2006). Ex vivo culture of human HSCs under hypoxia also stabilizes the hypoxia-inducible factor-1α (HIF-1α) protein, a master transcriptional regulator of the cellular and systemic hypoxia response, and several downstream effectors of HIF-1α (Danet et al., 2003). However, the regulatory mechanism and functional effects of BM hypoxia on HSCs in vivo has not been fully elucidated.

In the stem cell niche, HSCs are quiescent and show slow cell cycling. Various extracellular ligands, including CXCL12, angiopoietin-1, and/or thrombopoietin (TPO), contribute the quiescence of HSCs (Sugiyama et al., 2006; Arai et al., 2004; Yoshihara et al., 2007). Quiescent HSCs are maintained at a lower oxidative stress state to avoid their differentiation and exhaustion (Jang and Sharkis, 2007). HIF-1α is a bHLH-PAS-type transcriptional regulator. Under normoxic conditions, prolyl residues in the HIF-1α oxygen-dependent degradation domain (ODD) are hydroxylated by HIF prolyl hydroxylases (Phds) (Semenza, 2007; Simon and Keith, 2008). The hydroxylated ODD domain of HIF-1α protein is recognized by an E3 ubiquitin ligase, von Hippel-Lindau protein (VHL). In the autosomal-dominant hereditary disorder von Hippel Lindau disease, the VHL is mutated, resulting in overstabilized HIF-1α protein by the impaired ubiquitin proteasome pathway. Under hypoxic conditions, Phds are inactivated and HIF-1α protein escapes protein degradation. Several niche factors, such as TPO and stem cell factor (SCF), also stabilize HIF-1α protein in hematopoietic cells even under normoxia conditions (Kirito et al., 2005; Pedersen et al., 2008).

Stabilized HIF-1α protein forms a heterodimeric transcriptional complex with the oxygen-independent subunit HIF-1β, translocates to the nucleus, and directly binds hypoxia-responsive elements found in the promoter regions of numerous downstream regulators, thereby activating these regulators (Semenza, 2007; Simon and Keith, 2008). HIF-1β is reportedly required for hematopoietic cell generation during ontogeny (Adelman et al., 1999). However, a detailed analysis of the contribution of HIF-1α to the maintenance of adult HSCs has not yet

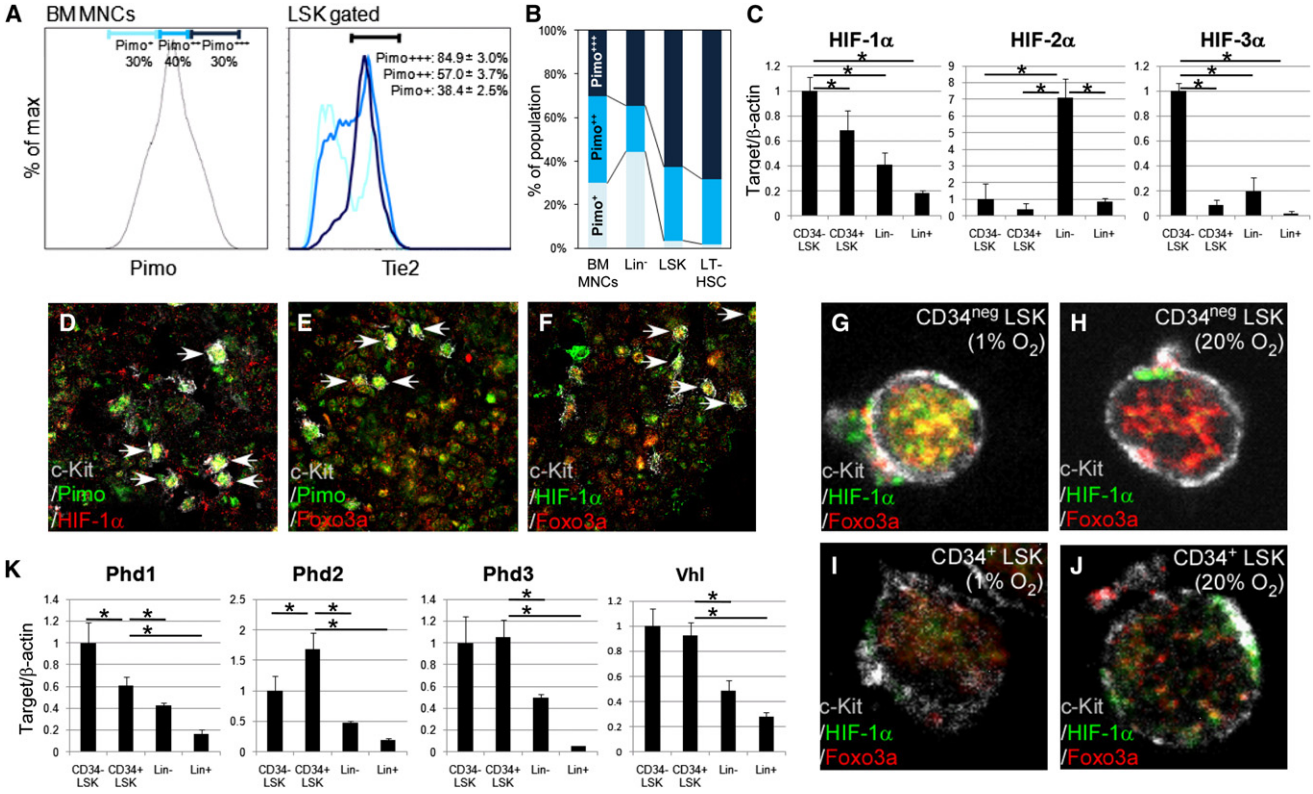

Figure 1. HSCs Are Hypoxic and Stabilize HIF-1α Protein

(A) FACS analysis of intracellular pimonidazole (Pimo) and the Tie2$^+$ fraction in Lineage marker$^-$ Sca-1$^+$ c-Kit$^+$ (LSK) cells. Intracellular Pimo was detected using an anti-Pimo-FITC antibody. Whole BM MNCs from 12-week-old wild-type mice were subdivided into three fractions (30%, 40%, and 30%, respectively) based on their Pimo fluorescence levels: highly (navy; Pimo^{+++}), moderately (blue; Pimo^{++}), or weakly (pale blue; Pimo$^+$) Pimo positive (left panel). The Tie2 expression in LSK-gated cells is shown in the right panel. Data represent the means ± SDs (n = 5).

(B) Oxygenation status of 12-week-old wild-type BM fractions, including BM MNCs, Lineage marker (Lin) $^-$, LSK, and LT-HSC (CD150$^+$ CD48$^-$ CD41$^-$ LSK). Pimo-positive BM fractions were determined as in (A). The total cell number was set to 100% and the relative percentage of individual fractions was calculated by flow cytometric analysis (n = 5).

(C) Expression of HIF-α family transcripts (HIF-1α, HIF-2α, and HIF-3α) in 10-week-old CD34$^-$ LSK, CD34$^+$ LSK, Lin$^-$, or Lin$^+$ cells. Each value was normalized to β-actin expression and is expressed as the fold induction compared to levels detected in CD34$^-$ LSK samples (mean ± SD, *$p < 0.05$, n = 4).

(D–F) Immunohistochemical analysis of the BM for c-Kit (gray), Pimo (green), and HIF-1α (red) (D); c-Kit (gray), Pimo (green), and Foxo3a (red) (E); or c-Kit (gray), HIF-1α (green), and Foxo3a (red) (F). Arrows indicate cells that are positive for both green and red signals in the nucleus of c-Kit$^+$ cells.

(G–J) Immunocytochemical detection of HIF-1α (green), Foxo3a (red), and c-Kit (gray) in HSCs (G and H) or progenitors (I and J) exposed to 12 hr of hypoxia (G and I) or normoxia (H and J) without cytokines. The preferential stabilization of HIF-1α was observed in HSCs under hypoxia.

(K) Expression of Phd1, Phd2, Phd3, and VHL transcripts in 10-week-old CD34$^-$ LSK, CD34$^+$ LSK, Lin$^-$, or Lin$^+$ cells. Each value was normalized to β-actin expression and is expressed as the fold induction compared to levels detected in CD34$^-$ LSK samples (mean ± SD, *$p < 0.05$, n = 4).

See also Figure S1.

been reported. Therefore, in the present study, we analyzed HSCs in HIF-1α- and VHL-deficient mice and found that the cellular pool and cell cycle status of HSCs were regulated by the HIF-1α level. Our analysis revealed that the regulation of the HIF-1α dose is critical for HSC maintenance in the hypoxic niche microenvironment of the BM.

RESULTS

HSCs Are Hypoxic in the Bone Marrow and Express HIF-1α Protein In Vivo

To analyze the intracellular oxygenation status of HSCs, we examined the uptake of the hypoxic cell marker pimonidazole (Pimo) by BM cells in vivo (Figure 1A). Intracellular incorporation of Pimo was analyzed by multicolor flow cytometry with a fluorescein (FITC)-conjugated anti-Pimo antibody 90 min after intravenous Pimo administration into mice. The BM MNCs were subdivided into highly (Pimo^{+++}; top 30% of BM MNCs), moderately (Pimo^{++}; middle 40% of BM MNCs), and weakly (Pimo$^+$; bottom 30% of BM MNCs) Pimo-positive fractions. The distribution of Tie2$^+$ cells in Lineage marker$^-$ Sca-1$^+$ c-Kit$^+$ cells (Tie2$^+$ LSK cells), which represent quiescent HSCs (Arai et al., 2004), was clearly enriched in the Pimo^{+++} fraction of BM MNCs (Figure 1A). The Pimo^{+++} fraction contained 68.2% of the LT-HSC (long-term reconstituting HSC) fraction that is made up of CD150$^+$ CD48$^-$ CD41$^-$ LSK cells, (Kiel et al., 2005) and 62.4% of the LSK fraction (Figure 1B). In sharp contrast, the Pimo$^+$ fraction only contained 1.8% of the CD150$^+$ CD48$^-$ CD41$^-$ LSK fraction and 3.5% of the LSK fraction (Figure 1B). Because 30% of the MNCs and 44.5% of the Lineage

marker-negative (Lin$^-$) cells were Pimo$^+$ (Figure 1B), we conclude that primitive hematopoietic cells, including CD150$^+$ CD48$^-$ CD41$^-$ LSK, Tie2$^+$ LSK, and LSK cells, are hypoxic in the BM in vivo.

Next, the mRNA expression levels of three HIF-α subunits, HIF-1α, -2α, and -3α, in CD34$^-$ LSK (the fraction of LT-HSC [Osawa et al., 1996], CD34$^+$ LSK (short-term reconstituting HSC; ST-HSC and multi-potent progenitor; MPP), Lin$^-$, and Lin$^+$ cells in 10-week-old BM were confirmed by quantitative PCR. The HIF-1α expression was higher in the more primitive fractions than in the differentiated fraction, and expression was highest in CD34$^-$ LSK cells (Figure 1C). Consistent with this, among the three homologs of the hypoxia-regulated HIF-α subunits, the online SAGE database SCDb (Hackney and Moore, 2005) shows the preferential expression of the HIF-1α transcript (SCDb ID: BMSB10895) in adult mouse HSCs (BM Rhodamine^{lo} Hoechst^{lo}) rather than in the differentiated cell fraction (Lin$^+$).

In our analysis, the expression level of HIF-2α mRNA in CD34$^-$ LSK cells was higher than in CD34$^+$ LSK cells. However, the highest expression among the four fractions was observed in Lin$^-$ cells. HIF-2α protein was mainly observed in the cytoplasm of CD34$^-$ LSK or CD34$^+$ LSK cells after hypoxic exposure ex vivo (Figure S1A available online). The expression level of the most uncharacterized HIF-α subunit, HIF-3α, was highest in the CD34$^-$ LSK fraction. Although the effect of HIF-3α on the cellular hypoxia response remains to be elucidated, HIF-3α itself is a direct transcriptional target of HIF-1α (Tanaka et al., 2009). Therefore, high HIF-3α expression levels in the CD34$^-$ LSK fraction implicate the preferential activation of HIF-1α in LT-HSCs.

To analyze the HIF-1α protein expression in situ, we performed immunohistochemical analysis of BM sections with anti-Pimo, anti-HIF-1α, and anti-Foxo3a antibodies. Foxo3a is a forkhead-type transcription factor that is essential for HSC quiescence (Tothova et al., 2007; Miyamoto et al., 2007). Because Foxo3a is only retained within LT-HSC nuclei and is excluded from ST-HSC/MPP nuclei, nuclear Foxo3a is a marker for quiescent HSCs (Miyamoto et al., 2007). More than 86.8% of the Pimo$^+$ c-Kit$^+$ cells possessed nuclear HIF-1α and Foxo3a (Figures 1D and 1E). Of the c-Kit$^+$ HIF-1α$^+$ cells, 95.4% had nuclear-localized Foxo3a, suggesting that the c-Kit$^+$ HIF-1α$^+$ Foxo3a$^+$ (KHF) cells were putative LT-HSCs in the BM (Figure 1F). In addition, 70.0% of the KHF cells localized to the endosteal zone of the BM, as reported previously (Kubota et al., 2008). Immunohistochemical analysis of the BM with SLAM markers (Kiel et al., 2005) revealed that these SLAM HSCs also expressed HIF-1α in vivo (Figure S1B).

We next examined the pure effect of hypoxia on HIF-1α protein stabilization. Isolated CD34$^-$ LSK or CD34$^+$ LSK cells were exposed to normoxia (20% O_2) or hypoxia (1% O_2) without cytokines for 12 hr, after which the c-Kit, HIF-1α, and Foxo3a protein levels were examined by immunocytochemistry (Figures 1G–1J). Stabilization of the nuclear HIF-1α protein was mainly observed in CD34$^-$ LSK cell samples exposed to hypoxia (Figure 1G). Levels of stabilized nuclear HIF-1α protein were relatively low in CD34$^-$ LSK cell samples exposed to normoxia and in CD34$^+$ LSK cell samples exposed to any oxygen tension (Figures 1H–1J). Effects of hypoxia and HIF-1α-stabilizing cytokines SCF and TPO on HIF-1α levels were examined by quantification of HIF-1α fluorescence intensity in LT-HSCs (CD34$^-$ Flt3$^-$ LSK) or CD34$^+$ LSK cells (Figure S1C). Without cytokines or hypoxic exposure, HIF-1α fluorescence intensity in LT-HSCs was higher than in CD34$^+$ LSK cells. Exposure to cytokines or hypoxia stabilized HIF-1α protein in LT-HSCs and CD34$^+$ LSK cells (Figure S1C). However, HIF-1α was highly stabilized in LT-HSC cells (Figure S1C). In contrast, cytokines induced HIF-1α stabilization more efficiently in CD34$^+$ LSK cells (Figure S1C).

The expression levels of Phd and VHL, the essential HIF-α degradation machinery, potentially help determine the set point for HIF-1α stabilization. To analyze the specific destabilization mechanism in CD34$^+$ LSK cells, we performed quantitative PCR analysis for Phds and VHL (Figure 1K). The expression level of Phd2 was higher in CD34$^+$ LSK cells than in CD34$^-$ LSK cells (Figure 1K). Of the Phd family members, Phd2 is the one most responsible for HIF-1α stabilization (Semenza, 2007). Thus, the higher Phd2 expression in CD34$^+$ LSK cells could be a regulatory mechanism for the preferential degradation of HIF-1α in CD34$^+$ LSK cells exposed to hypoxia. These data collectively suggest the specific contribution of HIF-1α to HSC maintenance in vivo.

Defective Maintenance of *HIF-1α$^{Δ/Δ}$* HSCs against Transplantation through *Ink4a/Arf*

We next examined the functional effect of HIF-1α on the quiescent state of HSCs by analyzing an inducible HIF-1α deletion model in vivo. To delete the HIF-1α gene from HSCs, we induced the Cre transgene in *Mx1-Cre:HIF-1α$^{flox/flox}$* mice (Ryan et al., 1998; Kuhn et al., 1995) by sequential polyI:polyC (pIpC) injections, which efficiently excised the *HIF-1α* gene from the hematological organs and peripheral blood (PB) cells (Figures S1D, S1E, S1H, and S1I). The deletion was maintained for at least 2 years in vivo (Figures S1H and S1I). In this mouse model (*HIF-1α$^{Δ/Δ}$* mice), the PB cell count and differentiation statuses of PB, thymus, spleen, and BM cells were maintained, except for a slight increase in leukocyte numbers and a reduction in the mean corpuscular volume (MCV) (Figures 2A and Figures S1F and S1G). Therefore, the overall differentiation capacity of *HIF-1α$^{Δ/Δ}$* HSCs was identical to that of *HIF-1α$^{+/+}$* HSCs at steady state.

We next assessed the progenitor capacity of *HIF-1α$^{Δ/Δ}$* BM MNCs. The conventional hematopoietic progenitor assays CFU-C and CFU-S_{12} revealed no significant difference between *HIF-1α$^{+/+}$* and *HIF-1α$^{Δ/Δ}$* BM MNCs (Figures S2A and S2B). In addition, the short-term (4 week) PB reconstitution abilities by sorted *HIF-1α$^{Δ/Δ}$* CD34$^+$ LSK cells transplanted into lethally irradiated Ly5.1 congenic recipients with Ly5.1 competitor cells were identical between the two genotypes (Figures S2C). Therefore, the short-term reconstitution ability of CD34$^+$ LSK cells (ST-HSCs and MPP cells) was normal under the *HIF-1α$^{Δ/Δ}$* condition.

We evaluated the stem cell capacity of *HIF-1α$^{Δ/Δ}$* HSCs by competitive BM transplantation (BMT). We transplanted 2000 LSK cells sorted from *HIF-1α$^{+/+}$* or *HIF-1α$^{Δ/Δ}$* mice into lethally irradiated Ly5.1 congenic recipients with Ly5.1 competitor cells. In 12-week-old *HIF-1α$^{Δ/Δ}$* mice (1–2 months after pIpC injection), the frequency of the LSK cells and the more primitive subfractions of LSK cells (CD150$^+$ CD48$^-$ CD41$^-$ LSK, Tie2$^+$ LSK, or CD34$^-$ Flt3$^-$ LSK cells) were similar to those in *HIF-1α$^{+/+}$* mice (Figure S2D). In primary recipients, the *HIF-1α$^{Δ/Δ}$* donor cells achieved significantly greater PB chimerism for up to 3 months

A

	HIF-1α$^{+/+}$	HIF-1α$^{\Delta/\Delta}$	P value
WBC(/ul)	5100±1400	7600±2100	0.027
RBC(x10^4/ul)	875±55	896±69	0.535
Hb(g/dl)	13.8±1.3	13.7±1.1	0.955
HCT(%)	46.0±2.7	45.3±2.9	0.635
MCV(fl)	52.6±0.7	50.6±1.0	0.001
MCH(pg)	15.7±0.7	15.3±0.5	0.250
Plt(x10^4/ul)	72.6±26.1	81.4±14.2	0.426

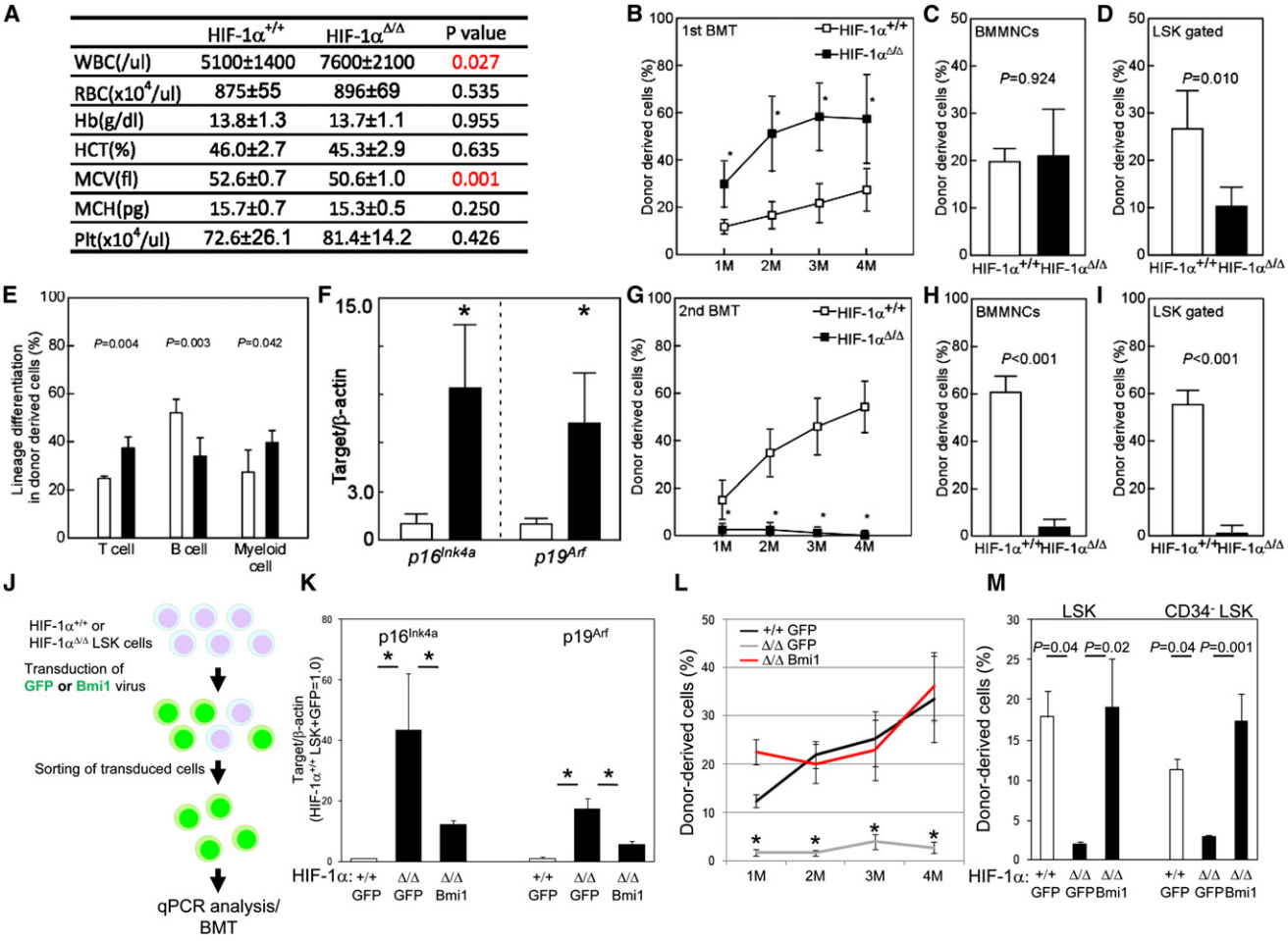

Figure 2. Defective Maintenance of *HIF-1α$^{\Delta/\Delta}$* HSCs against Transplantation through Ink4a/Arf

(A) Peripheral blood counts of *HIF-1α$^{+/+}$* or *HIF-1α$^{\Delta/\Delta}$* mice (mean ± SD, n = 24).

(B) PB chimerism in primary BMT recipients of *HIF-1α$^{+/+}$* (open boxes) or *HIF-1α$^{\Delta/\Delta}$* LSK (closed boxes) cells at the indicated times after BMT (mean ± SD, *p < 0.001, n = 10).

(C and D) Donor-derived (Ly5.2$^+$) BM MNC chimerism (C) or LSK chimerism (D) in primary BMT recipients of *HIF-1α$^{+/+}$* (open bars) or *HIF-1α$^{\Delta/\Delta}$* LSK (closed bars) cells 4 months after primary BMT (mean ± SD, n = 5).

(E) Differentiation status (CD4/CD8$^+$ T cells, B220$^+$ B cells, or Mac-1/Gr-1$^+$ myeloid cells) of donor-derived (Ly5.2$^+$) PB cells in primary BMT recipients of *HIF-1α$^{+/+}$* (open bars) or *HIF-1α$^{\Delta/\Delta}$* LSK (closed bars) cells (mean ± SD, n = 10).

(F) Quantitative PCR analysis of p16^{Ink4a} and p19^{Arf} in *HIF-1α$^{+/+}$* (open bars) or *HIF-1α$^{\Delta/\Delta}$* (closed bars) donor-derived LSK cells at 4 months after primary BMT (n = 4). Each value was normalized to β-actin expression and is expressed as the fold induction compared to levels detected in *HIF-1α$^{+/+}$* Ly5.2$^+$ LSK samples (mean ± SD, *p < 0.01).

(G) PB chimerism in secondary BMT recipients of *HIF-1α$^{+/+}$* (open boxes) or *HIF-1α$^{\Delta/\Delta}$* (closed boxes) Ly5.2$^+$ LSK cells at the indicated times after BMT (mean ± SD, *p < 0.001, n = 10).

(H and I) BM chimerism in secondary BMT recipients of *HIF-1α$^{+/+}$* (open bars) or *HIF-1α$^{\Delta/\Delta}$* (closed bars) LSK cells at 4 months after secondary BMT. Graphs show the donor-derived chimerism (Ly5.2$^+$) of BM MNCs (H) or LSK cells (I) (mean ± SD, n = 5).

(J) Study design of the suppression of Ink4a products by Bmi1 expression in *HIF-1α$^{\Delta/\Delta}$* LSK cells.

(K) Quantitative PCR analysis of *Ink4a* products (p16^{Ink4a} and p19^{Arf}) in LSK cells transduced with GFP or Bmi1 retrovirus for 48 hr in a *HIF-1α$^{+/+}$* or *HIF-1α$^{\Delta/\Delta}$* background (mean ± SD, n = 4, *p < 0.01).

(L) Donor-derived PB chimerism (Ly5.2$^+$) of *HIF-1α$^{+/+}$* or *HIF-1α$^{\Delta/\Delta}$* donor cells transduced with retroviruses carrying GFP or Bmi1 coding sequences at the indicated times after BMT (mean ± SEM, *p < 0.05 compared to other groups, n = 5).

(M) Donor-derived BM LSK or CD34$^-$ LSK chimerism (Ly5.2$^+$) of *HIF-1α$^{+/+}$* or *HIF-1α$^{\Delta/\Delta}$* donor cells transduced with retroviruses carrying GFP or Bmi1 coding sequences 4 months after BMT (mean ± SEM, n = 5).

See also Figure S2.

after BMT, and PB chimerism reached a plateau between 3 and 4 months after BMT (Figure 2B). Four months after BMT, recipients of the *HIF-1α$^{\Delta/\Delta}$* donor cells exhibited less chimerism than recipients of *HIF-1α$^{+/+}$* donor cells in the LSK-gated fraction of the BM (Figures 2C and 2D), indicating that the HSC levels were decreased. Spleens were also examined in the primary recipients at four months after BMT. However, no evidence for extramedullary hematopoietis was observed in *HIF-1α$^{\Delta/\Delta}$* HSC

recipients (Figure S2E). At this time, *HIF-1α*$^{\Delta/\Delta}$ donor-derived PB differentiation showed increased T and myeloid cell and reduced B cell counts (Figure 2E). Significant elevation of *Ink4a* transcription, a hallmark of senescent stem cells (Naka et al., 2008), was also detected in *HIF-1α*$^{\Delta/\Delta}$ LSK cells from primary BMT recipients (Figure 2F). We then isolated and transplanted 3000 primary donor-derived LSK cells into secondary recipients. A devastating loss in the long-term reconstitution ability of the *HIF-1α*$^{\Delta/\Delta}$ HSCs was seen in the PB and BM of the secondary recipient (Figures 2G–2I). Although surface marker analysis suggests that the frequency of various HSC fractions is within normal limits in young *HIF-1α*$^{\Delta/\Delta}$ mice (Figure S2D), the possibility exists that HSC contents within the LSK fraction before BMT are already compromised in *HIF-1α*$^{\Delta/\Delta}$ mice. To exclude this possibility, we prepared 1:1 BM chimera by transplanting pIpC-untreated *Mx1-cre:HIF-1α*$^{+/+}$ or *Mx1-cre:HIF-1α*$^{flox/flox}$ BM MNCs with identical numbers of CD45.1$^+$ CD45.2$^+$ competitor BM MNCs (Figure S2F). pIpC was intraperitoneally injected 4 months after BMT ("0 month" in Figure S2G). Before the pIpC injections, the PB repopulation unit (CD45.2$^+$ donor-derived chimerism [%]/CD45.1$^+$ CD45.2$^+$ competitor-derived chimerism [%]) was identical for the two genotypes (Figure S2G). Four months after the pIpC injection, the *HIF-1α*$^{\Delta/\Delta}$ PB repopulation unit overwhelmed *HIF-1α*$^{+/+}$ PB population in *HIF-1α*$^{+/+}$ recipients (Figure S2G). However, at 11 months after the pIpC injection, the level of the *HIF-1α*$^{\Delta/\Delta}$ PB repopulation had decreased below the level of the *HIF-1α*$^{+/+}$ PB repopulation unit. These data are consistent with the experimental phenotype of LSK BMT (Figures 2B and 2G) in primary recipients (4 months after pIpC in 1:1 BM chimera) and secondary recipients (11 months after pIpC in 1:1 BM chimera) and supports the progressive loss of *HIF-1α*$^{\Delta/\Delta}$ HSCs during BMT.

To directly analyze the impact of upregulated *Ink4a* products on *HIF-1α*$^{\Delta/\Delta}$ HSCs, we suppressed *Ink4a* products in *HIF-1α*$^{\Delta/\Delta}$ LSK cells by using the retroviral Bmi1 expression vector (Iwama et al., 2004) (Figure 2J). Isolated *HIF-1α*$^{\Delta/\Delta}$ LSK cells were transduced by control MSCV-IRES-EGFP retrovirus (GFP virus) or MSCV-Bmi1-IRES-EGFP retrovirus (Bmi1 virus) in an ex vivo culture with cytokines under normoxia. After transduction, the *HIF-1α*$^{\Delta/\Delta}$ LSK cells transduced with GFP virus showed significantly higher transcript levels of p16^{Ink4a} and p19^{Arf} than the *HIF-1α*$^{+/+}$ LSK cells transduced with GFP virus (Figure 2K). This observation confirmed the vulnerability of *HIF-1α*$^{\Delta/\Delta}$ LSK cells under stressed conditions (ex vivo culture) and following BMT (Figure 2F).

Transduction of the Bmi1 virus into *HIF-1α*$^{\Delta/\Delta}$ LSK cells suppressed the upregulation of *p16*^{Ink4a} and *p19*^{Arf} transcripts compared to *HIF-1α*$^{\Delta/\Delta}$ LSK cells transduced with GFP virus (Figure 2K). The sorting and transplantation of transduced cells revealed defects in PB repopulation and BM reconstitution after BMT in *HIF-1α*$^{\Delta/\Delta}$ LSK cells transduced with GFP virus (Figures 2L and 2M), which were significantly restored by the forced expression of Bmi1 in *HIF-1α*$^{\Delta/\Delta}$ LSK cells (Figures 2L and 2M). Collectively, these results indicate that the stem cell capacity, but not the progenitor capacity or productivity of differentiated *HIF-1α*$^{\Delta/\Delta}$ hematopoietic cells is impaired. Furthermore, other Bmi1 targets in HSCs, Pax5, and Ebf1 (Oguro et al., 2010) were not upregulated in *HIF-1α*$^{\Delta/\Delta}$ CD34$^-$ Flt3$^-$ LSK cells and were not suppressed by overexpression of Bmi1 (Figures S2H–S2J and data not shown); HIF-1α appears to play a protective role, mediated by *Ink4a* gene products, against senescence-induced HSC exhaustion. Because transplantation of wild-type CD45.1$^+$ BM MNCs into *HIF-1α*$^{+/+}$ or *HIF-1α*$^{\Delta/\Delta}$ mouse BM environments caused a decrease in short-term reconstitution (~2 months from BMT) and a loss of PB differentiation status, but not long-term reconstitution (4 months from BMT) (Figures S2K and S2L), defective maintenance of *HIF-1α*$^{\Delta/\Delta}$ HSCs under stress settings is mainly an cell-autonomous event.

Decreased Cellular Pool and Hypoxic Status of Aged *HIF-1α*$^{\Delta/\Delta}$ HSCs

We next examined the physiological stress resistance of *HIF-1α*$^{\Delta/\Delta}$ HSCs during aging. Aging significantly reduced the frequency (Figure 3A and Figure S2D) and number (Figure 3B) of putative HSCs (CD150$^+$ CD48$^-$ CD41$^-$ LSK, Tie2$^+$ LSK, or CD34$^-$ Flt3$^-$ LSK cells) in 56- to 74-week-old *HIF-1α*$^{\Delta/\Delta}$ mice compared to *HIF-1α*$^{+/+}$ mice. In 24-week-old *HIF-1α*$^{\Delta/\Delta}$ mice (i.e., when HSC loss has already started), more than 65% of the CD150$^+$ CD48$^-$ CD41$^-$ LSK or Tie2$^+$ LSK cells were Pimo^{+++} (Figures 3C and 3D) in accordance with the results in Figure 1A. The Pimo$^+$ fraction only contained less than 2% of the CD150$^+$ CD48$^-$ CD41$^-$ LSK or Tie2$^+$ LSK fraction (Figures 3C and 3D). Tie2$^+$ LSK or CD150$^+$ CD48$^-$ CD41$^-$ LSK cell loss was severe in the Pimo^{+++} fraction of *HIF-1α*$^{\Delta/\Delta}$ HSCs, and the Pimo$^+$ fraction was increased in Tie2$^+$ LSK cells and CD150$^+$ CD48$^-$ CD41$^-$ LSK cells (Figures 3C and 3D). Because the mean Pimo fluorescence and distribution in total BM MNCs was unchanged at this time (data not shown), the oxygenation status (Pimo^{+++}/Pimo^{++}/Pimo$^+$) in the *HIF-1α*$^{\Delta/\Delta}$ HSC pool might not depend on the overall BM oxygenation status, but on the HIF-1α-mediated intracellular oxygenation homeostasis of HSCs. These results suggest that HIF-1α, by modulating the oxygenation status of cells, critically regulates resistance to various stresses, including aging, in hypoxic mammalian HSCs. Moreover, in the aged *HIF-1α*$^{\Delta/\Delta}$ mice, we observed an increased number of LSK cells in the extramedullary site, spleen (Figure 3E). The red and white pulp structures of the spleen were disorganized in the aged *HIF-1α*$^{\Delta/\Delta}$ mice because of extracellular hematopoiesis (Figure 3F). Transplantation of 1×10^6 splenic MNCs rescued the lethally irradiated recipients (Figure 3G), which suggests that splenic LSK cells support the hematopoiesis of recipient mice.

Cell Cycle Regulation of HSCs and Hematopoietic Progenitors through HIF-1α

Sustaining cell cycle quiescence is an effective defense against stress in various species, organs, and individual cells, including mammalian HSCs (Arai et al., 2004). Therefore, to investigate the mechanism of HSC loss in *HIF-1α*$^{\Delta/\Delta}$ mice, we focused on the cell cycle of *HIF-1α*$^{\Delta/\Delta}$ HSCs. We sequentially injected the myelosuppressive agent 5-FU into mice. Sequential injections of a sublethal dose of 5-FU depletes cycling HSCs and causes quiescent HSCs to proliferate (Miyamoto et al., 2007). *HIF-1α*$^{\Delta/\Delta}$ mice showed significantly higher mortality rates than controls in response to myelosuppression by 5-FU (Figure 4A). This was primarily a hematopoietic cell-dependent event, given that recipient mice with BM from *HIF-1α*$^{\Delta/\Delta}$ mice also showed higher mortalities by 5-FU than controls (Figure S3A). The cell cycle

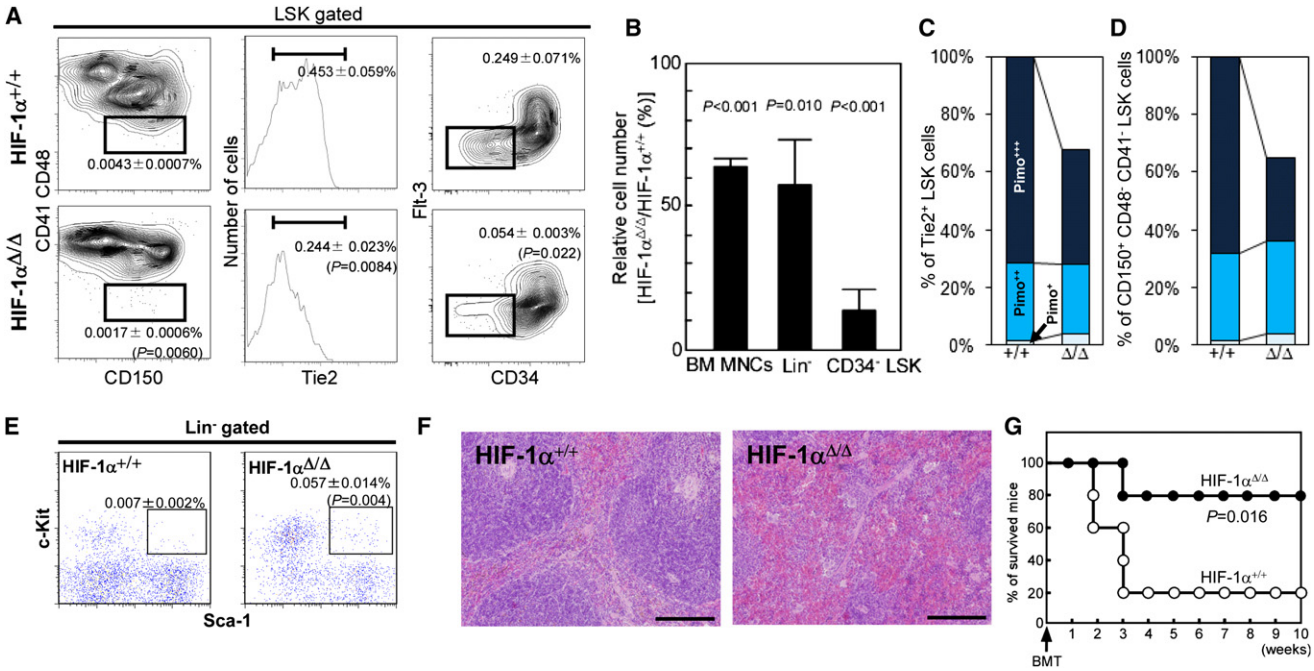

Figure 3. Loss and Altered Oxygenation Status of BM HSCs and Increased Extramedullar Hematopoiesis in Aged *HIF-1α*$^{\Delta/\Delta}$ Mice

(A) Flow cytometric analysis of various putative HSC fractions. FACS plots of *HIF-1α*$^{+/+}$ or *HIF-1α*$^{\Delta/\Delta}$ BM in 56- to 74-week-old mice. LT HSC (CD150$^+$ CD48$^-$ CD41$^-$ LSK cells; left column), LSK Tie2$^+$ (center column), and LSK Flt3$^-$ CD34$^-$ (right column) fractions are indicated. Numbers indicate the percentage of total BM MNCs (n = 6). Data represent the means ± SEMs.

(B) Relative cell numbers of BM MNCs, Lin$^-$ cells, and CD34$^-$ LSK cells in aged *HIF-1α*$^{\Delta/\Delta}$ mice (56–74 weeks) compared to aged *HIF-1α*$^{+/+}$ littermates (set to 100%) analyzed by flow cytometry (mean ± SEM, n = 6).

(C and D) Oxygenation status of 24-week-old BM Tie2$^+$ LSK cells (C) or CD150$^+$ CD48$^-$ CD41$^-$ LSK cells (D) subfractionated into highly (30%, navy; Pimo^{+++}), moderately (40%, blue; Pimo^{++}), or weakly (30%, pale blue; Pimo$^+$) Pimo-positive BM fractions, as in Figure 1A. The total cell number in *HIF-1α*$^{+/+}$ BM was set to 100%.

(E) Flow cytometric analysis of the splenic LSK fraction in aged *HIF-1α*$^{\Delta/\Delta}$ mice (56–74 weeks) compared to aged *HIF-1α*$^{+/+}$ littermates. LSK fraction is indicated. Numbers indicate the percentage of total BM MNCs (n = 4). Data represent the means ± SEMs.

(F) Histological examination of spleen from aged *HIF-1α*$^{\Delta/\Delta}$ mice (56–74 weeks) compared to aged *HIF-1α*$^{+/+}$ littermates. Representative pictures of spleen sections stained by hematoxylin and eosin. Scale bars represent 200 μm.

(G) Survival curves of lethally irradiated recipient mice transplanted with 1 × 10^6 mononuclear cells from aged *HIF-1α*$^{+/+}$ or *HIF-1α*$^{\Delta/\Delta}$ mouse spleens (n = 10).

kinetics of the *HIF-1α*$^{\Delta/\Delta}$ HSCs was directly examined by multicolor flow cytometry. Specific activation of the cell cycle, characterized by a reduction in the Ki67$^-$ G0 fraction and an increase in the Ki67$^+$ G1 fraction, was detected in *HIF-1α*$^{\Delta/\Delta}$ CD34$^-$ LSK cells by flow cytometric analysis (Figure 4B). Because the G0 phase in the CD34$^+$ LSK fraction was identical between the two genotypes (data not shown), the requirement of HIF-1α for cell cycle quiescence is mainly restricted to LT-HSCs.

Our HIF-1α loss of function results suggested that HIF-1α is essential for cell cycle regulation in HSCs. To verify this notion precisely, we prepared *Mx1-Cre:VHL*$^{+/flox}$, *Mx1-Cre:VHL*$^{flox/flox}$ mice and *Mx1-Cre:HIF-1α*$^{flox/flox}$ *VHL*$^{flox/flox}$ mice. Excision of one (*VHL*$^{+/\Delta}$ mice) or two (*VHL*$^{\Delta/\Delta}$ mice) alleles of the VHL gene by pIpC-induced Cre expression stabilized the HIF-1α protein in vivo in a VHL dose-dependent manner. The accumulation of HIF-1α protein was reversed by codeletion of HIF-1α with VHL (data not shown). However, pIpC injection into *Mx1-Cre:VHL*$^{flox/flox}$ or *Mx1-Cre:HIF-1α*$^{flox/flox}$ *VHL*$^{flox/flox}$ mice resulted in a 100% mortality rate within 1 week (data not shown). These deaths were hematopoiesis-independent events, given that BM replacement by wild-type MNCs in *Mx1-Cre:VHL*$^{flox/flox}$ or *Mx1-Cre:HIF-1α*$^{flox/flox}$ *VHL*$^{flox/flox}$ mice through BMT did not alter the results after pIpC injection (data not shown).

Therefore, we next analyzed the BM of *VHL*$^{+/\Delta}$ mice. *VHL*$^{+/\Delta}$ CD34$^-$ LSK cells showed an increase in G0 and S/G2/M phase cells, and a decrease in G1 phase cells (Figure 4C). Interestingly, the *VHL*$^{+/\Delta}$ CD34$^+$ LSK cells displayed an increased fraction of G0 phase and a reduced fraction of G1 phase cells (Figure 4D). These observations suggest that the increased dose of HIF-1α induced the G0 state in primitive hematopoietic cells, even in progenitor cells. CD34$^+$ LSK cells in *VHL*$^{+/\Delta}$ mice exhibited a higher quiescence induction efficiency (36.3% in *VHL*$^{+/+}$ versus 58.6% in *VHL*$^{+/\Delta}$) than CD34$^-$ LSK cells (79.0% in *VHL*$^{+/+}$ versus 88.7% in *VHL*$^{+/\Delta}$). This result is potentially due to the increased destruction of HIF-1α protein in hypoxic CD34$^+$ LSK cells in the presence of two alleles of the VHL gene, through Phd2-mediated hydroxylation (Figures 1G–1K).

These cell cycle phenotypes were also confirmed by Pyronin Y staining or short-term BrdU labeling. In Pyronin Y analysis, *HIF-1α*$^{\Delta/\Delta}$ CD34$^-$ LSK cells but not CD34$^+$ LSK cells showed a decreased Pyronin Y- quiescent fraction (Figures S3B–S3D). In contrast, *VHL*$^{+/\Delta}$ CD34$^+$ LSK cells but not CD34$^-$ LSK cells

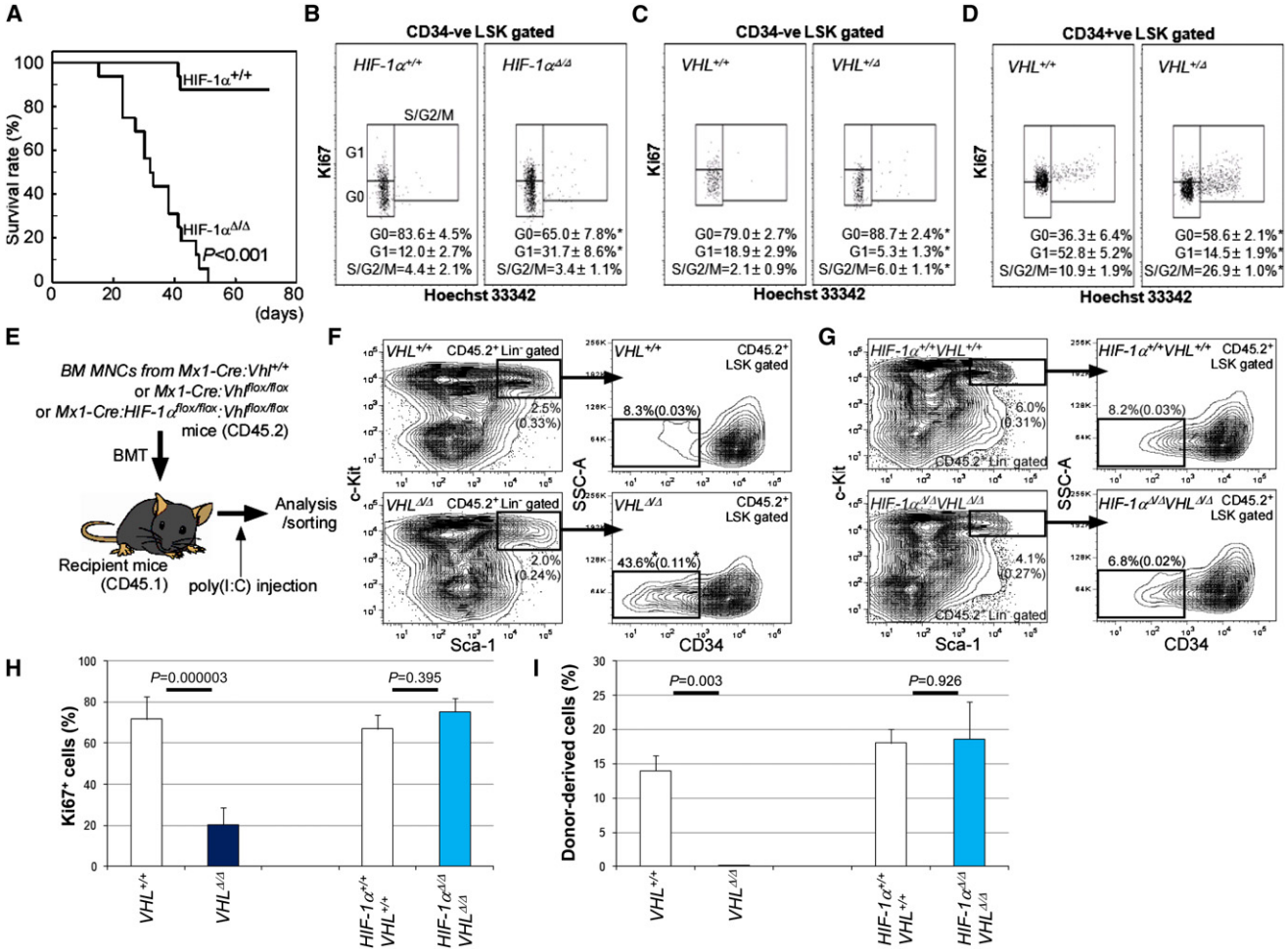

Figure 4. HIF-1α Dose-Dependent Regulation of Cell Cycle, Cell Number, and HSC Ability In Vivo

(A) Survival in response to sequential myelosuppressions (5-FU, 150 mg/kg at 10 day intervals) in *HIF-1α*$^{+/+}$ or *HIF-1α*$^{\Delta/\Delta}$ mice (n = 16).

(B–D) Flow cytometric analysis of the cell cycle in the CD34^{-}-LSK fraction from *HIF-1α*$^{+/+}$ or *HIF-1α*$^{\Delta/\Delta}$ mice (B), and the CD34^{-} LSK (C) or CD34^{+} LSK (D) fractions from *VHL*$^{+/+}$ or *VHL*$^{+/\Delta}$ mice (mean ± SD, n = 6; *p < 0.002).

(E) Schematic diagram of the *VHL*$^{\Delta/\Delta}$ or *HIF-1α*$^{\Delta/\Delta}$*:VHL*$^{\Delta/\Delta}$ BM mouse models.

(F and G) Flow cytometric analysis of the BM HSC fraction in *VHL*$^{\Delta/\Delta}$ (F) or *HIF-1α*$^{\Delta/\Delta}$*:VHL*$^{\Delta/\Delta}$ (G) BM mice and controls. Numbers indicate the mean percentage of gated cells. Amounts in parentheses indicate the mean percentage of all donor-derived BM MNCs (n = 5, *p < 0.01).

(H) Quantification of the proportion of Ki67-positive cells in LSK cells assessed by immunocytochemistry. A significant reduction in the Ki67-positive cell fraction was observed in *VHL*$^{\Delta/\Delta}$ LSK cells, but not in *HIF-1α*$^{\Delta/\Delta}$*: VHL*$^{\Delta/\Delta}$ LSK cells compared to controls. Data represent the means ± SD.

(I) PB chimerism of *VHL*$^{+/+}$, *VHL*$^{\Delta/\Delta}$, *HIF-1α*$^{+/+}$*:VHL*$^{+/+}$, and *HIF-1α*$^{\Delta/\Delta}$*:VHL*$^{\Delta/\Delta}$ donor–derived LSK cells (2000 cells) transplanted into lethally irradiated Ly5.1 congenic recipients with Ly5.1 competitor cells 4 months after BMT (mean ± SEM, n = 5).

See also Figure S3.

showed an increased Pyronin Y^{-} quiescent fraction (Figures S3B–S3D). Also, short-term BrdU labeling demonstrated that cycling cells were high in the *HIF-1α*$^{\Delta/\Delta}$ CD34^{-} LSK population but not in the *HIF-1α*$^{\Delta/\Delta}$ CD34^{+} LSK cell population (Figures S3E and S3F). In *VHL*$^{+/\Delta}$ mice, a decreased cycling status was only observed in *VHL*$^{+/\Delta}$ CD34^{+} LSK cells (Figures S3E and S3F).

To overcome the difficulty in deleting two alleles of the VHL gene in HSCs, we prepared recipient mice with pIpC-untreated *Mx1-Cre:VHL*$^{flox/flox}$ BM MNCs or *Mx1-Cre:HIF-1α*$^{flox/flox}$ *VHL*$^{flox/flox}$ BM MNCs (Figure 4E). Deletion of the VHL gene by pIpC injections after BMT induced stabilization of the HIF-1α protein in the nucleus in ~97% of LSK cells, and no death was observed following pIpC injections (data not shown). Analysis of the BM showed that there was no significant change in the LSK fraction and significant accumulation of CD34^{-} LSK cells in the *VHL*$^{\Delta/\Delta}$ BM model (Figure 4F). This effect was HIF-1α dependent, given that codeletion of *HIF-1α* and *VHL* in the *HIF-1α*$^{\Delta/\Delta}$*:VHL*$^{\Delta/\Delta}$ BM model prevented the accumulation of CD34^{-} LSK cells (Figure 4G). Analysis of the LSK fraction showed that a significant reduction in Ki67^{+} (i.e., non-G0) cells occurred in *VHL*$^{\Delta/\Delta}$ LSK cells (Figure 4H), but not in *HIF-1α*$^{\Delta/\Delta}$*:VHL*$^{\Delta/\Delta}$ LSK cells (Figure 4H). Therefore, in addition to the accumulation of phenotypical HSCs in the *VHL*$^{\Delta/\Delta}$ BM model, induction of cell cycle quiescence was also HIF-1α dependent.

Because a low expression of CD34 in LSK cells is not only a feature of functional HSCs but also a hallmark of attenuated

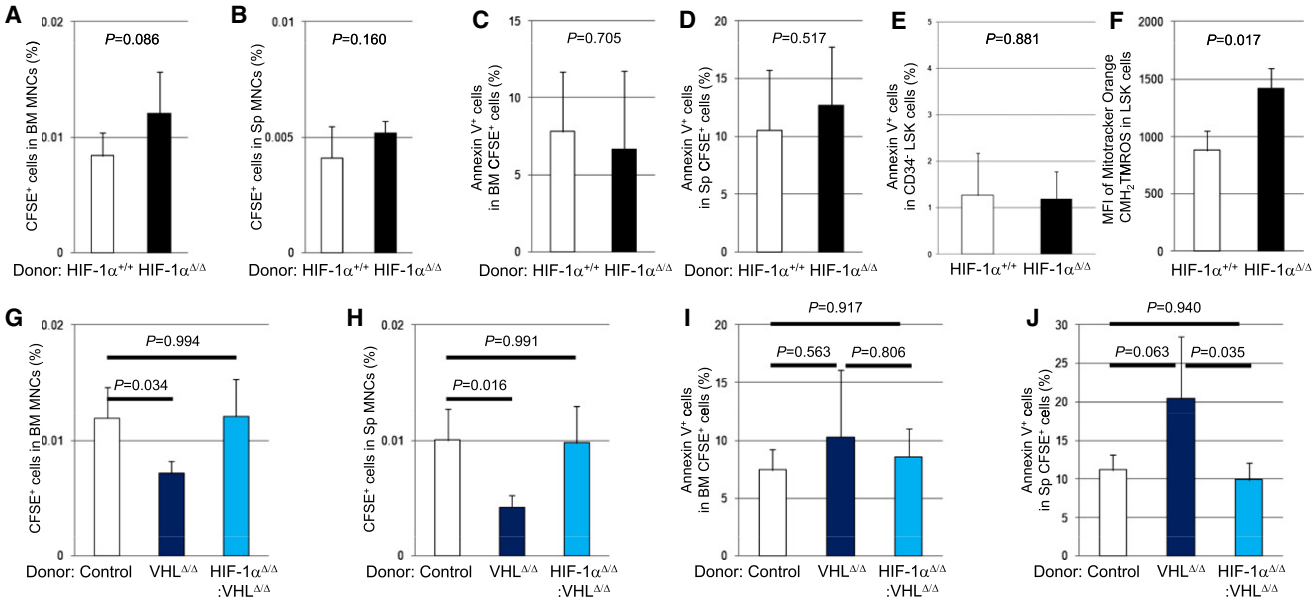

Figure 5. Homing Capacity and Apoptosis in *HIF-1α*$^{\Delta/\Delta}$ or *VHL*$^{\Delta/\Delta}$ HSCs

(A and B) Homing capacity of CFSE-labeled 2 × 10^5 Lin- Sca-1$^+$ cells from *HIF-1α*$^{+/+}$ or *HIF-1α*$^{\Delta/\Delta}$ mice to BM (A) or spleen (B) 16 hr after BMT (n = 5, mean ± SD).
(C and D) Annexin V$^+$ apoptotic cells in CFSE$^+$ transplanted *HIF-1α*$^{+/+}$ or *HIF-1α*$^{\Delta/\Delta}$ Lin$^-$ Sca-1$^+$ cells 16 hr after BMT (n = 5, mean ± SD).
(E) Annexin V$^+$ apoptotic cells in *HIF-1α*$^{+/+}$ or *HIF-1α*$^{\Delta/\Delta}$ BM CD34$^-$ LSK cells (n = 4, mean ± SD).
(F) Redox-sensitive MitoTracker fluorescence in *HIF-1α*$^{+/+}$ or *HIF-1α*$^{\Delta/\Delta}$ BM CD34$^-$ LSK cells (n = 3, mean ± SD).
(G and H) Homing capacity of CFSE-labeled 2 × 10^5 Lin$^-$ Sca-1$^+$ cells from control wild-type BM, *VHL*$^{\Delta/\Delta}$ BM, or H*IF-1α*$^{\Delta/\Delta}$*:VHL*$^{\Delta/\Delta}$ BM mice to BM (G) or spleen (H) 16 hr after BMT (n = 4–5, mean ± SD).
(I and J) Annexin V$^+$ apoptotic cells in CFSE$^+$ transplanted Lin$^-$ Sca-1$^+$ cells from control wild-type BM, *VHL*$^{\Delta/\Delta}$ BM, or *HIF-1α*$^{\Delta/\Delta}$*:VHL*$^{\Delta/\Delta}$ BM mice to BM (I) or spleen (J) 16 hr after BMT (n = 4–5, mean ± SD).

HSCs (Sudo et al., 2000), we tested the transplantation capacity of *VHL*$^{\Delta/\Delta}$ LSK cells. Isolated *VHL*$^{+/+}$ LSK, *VHL*$^{\Delta/\Delta}$ LSK, *HIF-1α*$^{+/+}$*:VHL*$^{+/+}$ LSK, or *HIF-1α*$^{\Delta/\Delta}$*:VHL*$^{\Delta/\Delta}$ LSK donor-derived cells (2000 cells) were transplanted into lethally irradiated Ly5.1 congenic recipients with Ly5.1 competitor cells. The PB reconstitution ability of *VHL*$^{\Delta/\Delta}$ LSK cells was severely impaired in recipients 4 months after BMT (Figure 4I). This was dependent on HIF-1α, given that *HIF-1α*$^{\Delta/\Delta}$*:VHL*$^{\Delta/\Delta}$ LSK cells achieved a PB chimerism comparable to the control (Figure 4I). The *HIF-1α*$^{\Delta/\Delta}$*:VHL*$^{\Delta/\Delta}$ donor-derived cells also had multilineage reconstitution capacities (data not shown). The CD150$^+$ CD48$^-$ CD41$^-$ LSK fraction decreased in the *VHL*$^{\Delta/\Delta}$ BM mouse (Figure S3G). Because there was no significant difference in the frequency of CD150$^+$ CD48$^-$ CD41$^-$ LSK in *HIF-1α*$^{\Delta/\Delta}$*:VHL*$^{\Delta/\Delta}$ BM mice (Figure S3G), the decreased HSC level after biallelic loss of *VHL* is considered to be a HIF-1α-dependent event. Therefore, in addition to the loss of HIF-1α function in HSCs, HIF-1α overexpression also induces abnormal cell cycle kinetics and suppresses the stem cell ability in vivo. These data demonstrate that precise regulation of the HIF-1α dose is critical to maintaining cell cycle kinetics and the HSC capacity during BMT in primitive hematopoietic cells.

Homing Capacity, Apoptosis, and ROS Production in *HIF-1α*$^{\Delta/\Delta}$ or *VHL*$^{\Delta/\Delta}$ HSCs

To characterize the repopulation defect in *HIF-1α*$^{\Delta/\Delta}$ or *VHL*$^{\Delta/\Delta}$ HSCs, we tested the homing capacity and viability of *HIF-1α*$^{\Delta/\Delta}$ or *VHL*$^{\Delta/\Delta}$ progenitors after transplantation. First, *HIF-1α*$^{\Delta/\Delta}$ Lin$^-$ Sca-1$^+$ primitive BM cells were sorted, CFSE-labeled, and transplanted into lethally irradiated recipients. Sixteen hours after BMT, recipient BM and spleen were analyzed. Homing capacity and apoptotic cell ratio of transplanted CFSE$^+$ cells in BM or spleen were equivalent in the two genotypes (Figures 5A–5D). Annexin V$^+$ apoptotic cells in *HIF-1α*$^{\Delta/\Delta}$ HSC were also unchanged at the static state (Figure 5E). Therefore, the repopulation defect of *HIF-1α*$^{\Delta/\Delta}$ HSCs cannot be attributed to homing or a cell survival defect. Because an increased production of ROS, an inducer of cell cycling and senescence in HSCs (Miyamoto et al., 2007), was observed in *HIF-1α*$^{\Delta/\Delta}$ CD34$^-$ *LSK* cells (Figure 5F), the ROS-mediated overproliferation of *HIF-1α*$^{\Delta/\Delta}$ HSCs could account for the loss of their stem cell characteristics through senescence-associated events.

In sharp contrast, defective homing to the BM and spleen was observed in *VHL*$^{\Delta/\Delta}$ Lin$^-$ Sca-1$^+$ primitive BM cells (Figures 5G and 5H). The apoptotic cell ratio in transplanted cells was suppressed by codeletion of *HIF-1α* in *VHL*$^{\Delta/\Delta}$ cells homed to the spleen, but not to the BM (Figures 5I and 5J). These observations suggest that, in addition to suppression of the cell cycle, *VHL*$^{\Delta/\Delta}$ HSCs lose their stem cell capacity in part through defective homing and increased apoptosis of transplanted cells with an aberrantly high level of HIF-1α

Loss of One *VHL* Allele Ameliorated Stress Resistance of HSCs during Aging or BMT

The loss of two alleles of *VHL* resulted in a transplantation defect through HIF-1α overstabilization (Figures 4I and 5G–5J).

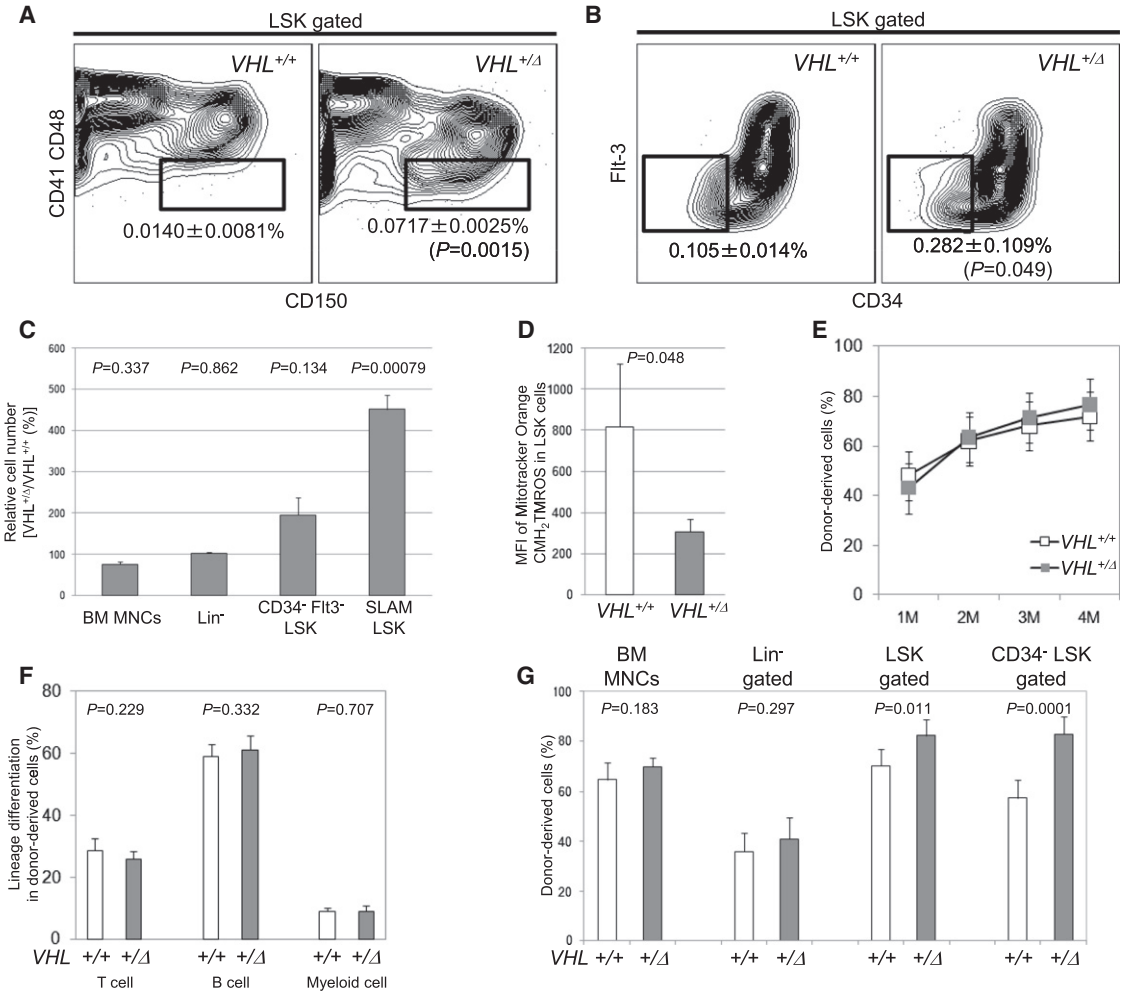

Figure 6. Analysis of *VHL*$^{+/\Delta}$ HSCs upon Aging or Transplantation

(A and B) Flow cytometric analysis of putative HSC fractions. FACS plots of *VHL*$^{+/+}$ or *VHL*$^{+/\Delta}$ BM in one-year-old mice. LT HSC (CD150^{+} CD48^{-} CD41^{-} LSK) (A) or LSK Flt3^{-} CD34^{-} (B) fractions are indicated. Numbers indicate the percentage of total BM MNCs (n = 3). Data represent the means ± SDs.

(C) Relative cell numbers of BM MNCs, Lin^{-} cells, CD34^{-} Flt3^{-} LSK cells, and CD150^{+} CD48^{-} CD41^{-} LSK cells in aged *VHL*$^{+/\Delta}$ mice (1 years old) compared to aged VHL$^{+/+}$ littermates (set to 100%) as analyzed by flow cytometry (mean ± SEM, n = 3).

(D) Redox-sensitive MitoTracker fluorescence in 1-year-old *VHL*$^{+/+}$ or *VHL*$^{+/\Delta}$ BM CD150^{+} CD48^{-} CD41^{-} LSK cells (n = 3, mean ± SD).

(E) PB chimerism in primary BMT recipients of *VHL*$^{+/+}$ (white boxes) or *VHL*$^{+/\Delta}$ LSK (gray boxes) cells at the indicated times after BMT (mean ± SD, n = 5).

(F) Differentiation status (CD4/CD8^{+} T cells, B220^{+} B cells, or Mac-1/Gr-1^{+} myeloid cells) of donor-derived (Ly5.2^{+}) PB cells in primary BMT recipients of *VHL*$^{+/+}$ or *VHL*$^{+/\Delta}$ LSK cells (mean ± SD, n = 5).

(G) Donor-derived (Ly5.2^{+}) BM MNC, Lin^{-}, LSK, or CD34^{-} LSK chimerism in primary BMT recipients of *VHL*$^{+/+}$ or *VHL*$^{+/\Delta}$ LSK cells 4 months after BMT (mean ± SD, n = 5).

See also Figure S4.

Although the PB cell count in *VHL*$^{\Delta/\Delta}$ BM mouse was equivalent to that in the control (Figure S4A), the PB differentiation status was also attenuated in *VHL*$^{\Delta/\Delta}$ BM mice (Figure S4B). This could be potentially due to the hyperactivation of HIF-1α in HSCs. To investigate the optimal HIF-1α dose in vivo, we employed the loss of one VHL allele for stress resistance of HSCs, which showed enhanced quiescence in the HSC and progenitor fraction (Figures 4C and 4D) and normal PB differentiation capacity (Figure S4C). Aged (one-year-old) *VHL*$^{+/+}$ or *VHL*$^{+/\Delta}$ BM showed a significant increase in CD150^{+} CD48^{-} CD41^{-} LSK and CD34^{-} Flt3^{-} LSK frequencies upon the deletion of one VHL allele (Figures 6A and 6B). A significant increase of CD150^{+} CD48^{-} CD41^{-} LSK cell number and a tendency for a greater CD34^{-} Flt3^{-} LSK cell number in *VHL*$^{+/\Delta}$ BM were also observed (Figure 6C). At this time, ROS generation in the CD150^{+} CD48^{-} CD41^{-} LSK fraction was suppressed in *VHL*$^{+/\Delta}$ mice (Figure 6D). Next, to test the resistance of *VHL*$^{+/\Delta}$ HSCs to BMT stress, we transplanted 12-week-old *VHL*$^{+/\Delta}$ LSK cells, which had an identical number and frequency of HSCs compared to wild-type LSK cells (data not shown), into lethally irradiated recipients with competitor cells. PB chimerism was comparable between *VHL*$^{+/+}$ or *VHL*$^{\Delta/\Delta}$ cell recipients (Figure 6E). Although the differentiation status of the donor-derived PB cells was also identical (Figure 6F), BM chimerism of the LSK or CD34^{-}

LSK fraction was significantly improved (Figure 6G). Collectively, the loss of one *VHL* allele ameliorated HSC maintenance under stress conditions, such as aging and BMT.

DISCUSSION

Critical regulation of HSC cell cycle quiescence by HIF-1α has important implications for understanding the regulation of stem cell homeostasis by the microenvironment. In the present study, we investigated the role of the relatively hypoxic nature of HSCs among BM cells, and clarified the significance of that hypoxia in modulating HSC quiescence through the HIF-1α/VHL regulatory system. The HIF-1α protein is preferentially expressed in LT-HSCs, probably because HIF-1α mRNA is preferential expressed in $CD34^-$ LSK cells (Figure 1C). In addition, a specific HIF-1α degradation mechanism in $CD34^+$ LSK cells could exist even under hypoxia or cytokine stimulation. A higher level of expression of *Phd2* in $CD34^+$ LSK might account for the mechanism (Figure 1K). Also, the differential responses to cytokines or hypoxia in LT-HSCs and $CD34^+$ LSK cells suggest that the signal transduction pathway that transduces cytokines or hypoxia signals to induce HIF-1α stabilization are different in these cells (Figure S1C). Consistent with the hypothesis that the entry of HSCs into the cell cycle influences their life span, we found that the fraction of quiescent HSCs decreased and that *HIF-1α*$^{\Delta/\Delta}$ HSCs were lost during stressed conditions, including serial transplantation and aging. The Ink4a locus, which produces $p16^{Ink4a}$ and $p19^{Arf}$ transcripts, is known to contribute to the aging and exhaustion of HSCs (Naka et al., 2008). LSK chimerism was decreased in primary recipients in an Ink4a-dependent manner. Suppression of Ink4a products by Bmi1 induced the recovery of PB and BM repopulation in recipient mice. During the process of aging, HSCs decreased in number in the BM, lost their hypoxic nature, and showed extramedullary hematopoiesis. Conventional HIF-1 targets, including *Vegfa*, *Epo*, and *Cxcr4*, were not dysregulated in *HIF-1α*$^{\Delta/\Delta}$ mice (Figures S2M–S2P). Bmi1 is essential for proper oxygen metabolism in mitochondria (Liu et al., 2009). Therefore, it may be that the observed Bmi1-mediated rescue of the BM repopulation ability in *HIF-1α*$^{\Delta/\Delta}$ HSCs was partly regulated by the metabolic pathway. Overall, HIF-1α plays multiple unique roles for the proper maintenance of HSCs in vivo.

HSCs, which have few mitochondria, may remain quiescent in the cell cycle by using anaerobic metabolism in the hypoxic endosteal zone (Parmar et al., 2007; Kim et al., 1998). HIF-1α is an essential regulator for cellular metabolic adaptation to hypoxia (Semenza, 2007). Because HSCs have relatively fewer mitochondria than proliferating progenitors (Kim et al., 1998), anaerobic respiration, low oxygen consumption, and low ROS production regulated by HIF-1α might comprise an effective survival strategy for BM HSCs under conditions of limited oxygen supply. In our preliminary data, glycolytic pathways were predominant in the energy metabolism of wild-type HSCs, whereas gene expression levels of *Glut1* (a transporter for glucose intake) and pyruvate dehydrogenase kinase (*Pdk*) were downregulated in the HSCs of *HIF1α*$^{\Delta/\Delta}$ mice. These data suggest that glycolytic pathway regulation by HIF-1α is critical for the maintenance of quiescent HSCs (K.T. and T.S., unpublished data).

In contrast to *HIF-1α*$^{\Delta/\Delta}$ HSCs, deletion of one or two alleles of VHL stabilized the HIF-1α protein and induced HSC quiescence in a HIF-1α dose-dependent manner. Interestingly, in addition to the HSCs, the progenitor fraction of *VHL*$^{+/\Delta}$ mice also became quiescent. In our analysis, the cell cycle status of *HIF-1α*$^{\Delta/\Delta}$ progenitors was identical to controls. Therefore, normal progenitors do not constitutively stabilize HIF-1α in vivo, but can utilize HIF-1α protein to become quiescent. Because rapid progenitor proliferation is required for proper hematopoiesis, specific HIF-1α destruction mechanisms in progenitors are important, as is the relatively nonhypoxic nature of progenitors. These data confirm the significance of the HIF-1α-mediated oxygen metabolism changes and characterize HSCs and progenitors in terms of the cell cycle. Overstabilization of the HIF-1α protein in *VHL*$^{\Delta/\Delta}$ BM mice also perturbed the ability of HSCs during BMT; this was mediated in part by a homing defect and an attenuated viability during BMT (Figure 5). This is consistent with the previous finding that the forced expression of GATA2, an essential regulator of HSC quiescence, results in loss of stem cell capacity in human HSCs (Tipping et al., 2009). Recently, it was reported that *Cited2*, a negative regulator for HIF-1α, selectively maintains adult HSC functions, at least in part, via *Ink4a/Arf* and *Trp53* (Kranc et al., 2009). Collectively, these data indicate that precise regulation of the appropriate HIF-1α dose in HSCs is essential for determining the cell cycle status and stem cell capacity of HSCs. In support of this, loss of one VHL allele preferentially affected HSCs during aging and BMT (Figure 6).

Hypoxic quiescent HSCs are dispersed, and do not accumulate, in the theoretically hypoxic BM endosteal zone (Figures 1D–1F). This BM zone is highly vascularized, and transplanted HSCs attach to endothelial cells and leave the vasculature to migrate deep into the BM (sometimes near the osteoblastic cells) (Lo Celso et al., 2009; Xie et al., 2009). The putative HSCs with an intracellular hypoxic status included the less-differentiated $Tie2^+$ LSK or $CD150^+$ $CD48^-$ $CD41^-$ LSK cells (Figures 1B, 3C, and 3D). Because $CD150^+$ $CD48^-$ $CD41^-$ LSK cells were originally identified as vasculature-associated cells (Kiel et al., 2005), the HSC oxygenation status has been proposed to be independently regulated by the association of these cells with the vasculature. In support of this hypothesis, loss of HIF-1α affected the intracellular oxygenation status of HSCs (Figures 3C and 3D).

The critical role for HIF-1α in HSC cell cycle regulation broadens the concept of stem cell niche involvement in the oxygenation status. It also implies a strategy for maintaining and expanding HSC resources based on cellular oxygen metabolism reprogramming, including the modulation of HSC quiescence through the cell oxygenation status of HIF-1α.

EXPERIMENTAL PROCEDURES

Mice

HIF-1α$^{flox/flox}$ (Ryan et al., 1998) or *VHL*$^{flox/flox}$ mice (Haase et al., 2001) were crossed to the C57BL/6 background for more than ten generations and were mated to interferon-inducible Mx1-cre transgenic mice (Kuhn et al., 1995) for generation of *Mx1-cre:HIF-1α* $^{flox/flox}$ or *Mx1-cre:VHL*$^{flox/flox}$ mice. Offspring of these mice were genotyped by PCR-based assays with DNA from mouse tail snips. To prepare *HIF-1α*$^{\Delta/\Delta}$ mice, Mx1-cre expression was induced by intraperitoneal injection of 400 μg of pIpC (Amersham), on three alternate days, into 4- to 8-week-old mice. At least 4 weeks after pIpC

injection, 10 to 12-week-old mice were used in each experiment, unless stated otherwise. We utilized age-matched pIpC-injected *Mx1-cre:HIF-1α*$^{+/+}$ or *Cre (-):HIF-1α* $^{flox/flox}$ mice as controls (HIF-1α$^{+/+}$ mice). C57BL/6-Ly5.1 congenic or C57BL/6-Ly5.1/Ly5.2 F1 mice were used for competitive repopulation assays.

To prepare mice with *VHL*$^{\Delta/\Delta}$ or *HIF-1α*$^{\Delta/\Delta}$*:VHL*$^{\Delta/\Delta}$ BM (*VHL*$^{\Delta/\Delta}$ or *HIF-1α*$^{\Delta/\Delta}$*:VHL*$^{\Delta/\Delta}$ BM mice), we transplanted (0.6-1) × 10^7 BM MNCs or CD45$^+$ BM MNCs from *Mx1-cre:VHL*$^{flox/flox}$ or *Mx1-cre:HIF-1α* $^{flox/flox}$: *VHL*$^{flox/flox}$ mice into lethally irradiated C57BL/6-Ly5.1 mice. We checked for PB chimerism 6 weeks after BMT and utilized recipients with >90% donor-derived cells. Cre expression in the replaced BM was induced by intraperitoneal injection of 250 μg of pIpC (Amersham) on three alternate days. We used *Mx1-cre:HIF-1α*$^{+/+}$*:VHL*$^{+/+}$ BM mice as controls (*VHL*$^{+/+}$ BM mice). For blood count analysis, PB from the postorbital vein was collected in heparinized microtubes (Drummond Scientific) and analyzed using CellTac (Nihon Kohden). All procedures were performed in accordance with the guidelines of Keio University School of Medicine.

Flow Cytometry

Analysis of various HSC fractions were essentially performed as previously described (Arai et al., 2004).

Immunocytochemistry and Immunohistochemistry

Immunocytochemistry with isolated cells was performed as described previously (Takubo et al., 2008). For preparation of cultured cells, sorted cells were incubated under normoxia (20% O_2) or hypoxia (1% O_2) for 12 hr in serum-free SF-O3 medium (Sanko Jyunyaku). For histological BM examination, fresh frozen BM sections (6 μm thickness) of the femoral bone were prepared with a cryostat equipped with a tungsten blade (Microedge Instruments). Sections were placed onto MAS-coated glass slides (Matsunami Glass), dried completely, and fixed with 4% PFA for 10 min, and subsequently stained with antibody. Care was taken to avoid any detachment of the bony portion.

Bone Marrow Transplants, Progenitor Assays, and Peripheral Blood Analysis

LSK cells from *HIF-1α*$^{+/+}$ or *HIF-1α*$^{\Delta/\Delta}$ mice (Ly5.2), together with 4 × 10^5 BM MNCs from C57Bl/6-Ly5.1 mice, were transplanted into lethally irradiated C57Bl/6-Ly5.1 congenic mice. Secondary transplantations into lethally irradiated C57Bl/6-Ly5.1 congenic mice were performed with Ly5.2$^+$ LSK cells from primary recipients, together with 4 × 10^5 BM MNCs from C57Bl/6-Ly5.1 mice. Recipient mice were sacrificed for analysis 4 months after BMT. For splenic cell transplantation, 1 × 10^6 splenic MNCs from *HIF-1α*$^{+/+}$ or *HIF-1α*$^{\Delta/\Delta}$ mice (Ly5.2) were transplanted into lethally irradiated C57Bl/6-Ly5.1 congenic mice. Examination of the progenitor capacity by CFU-C, CFU-S_{12}, and BMT with CD34$^+$ LSK cells was performed as previously described (Miyamoto et al., 2007).

Statistical Analysis

Data are presented as the means ± SD, unless stated otherwise. Statistical significance was determined by Tukey's multiple comparison test. For comparison of a two-group experiment, the two-tailed Student's t test was used with the exception of the 5-FU survival assay and BMT assay with splenic MNCs, which were analyzed with the log-rank test.

SUPPLEMENTAL INFORMATION

Supplemental Information includes Supplemental Experimental Procedures and four figures and can be found with this article online at doi:10.1016/j.stem.2010.06.020.

ACKNOWLEDGMENTS

We thank T. Kitamura for providing Plat E packaging cells; A. Iwama for providing Bmi1 retroviral vector; K. Rajewsky for providing *Mx1-Cre* mice; V. Haase for providing *VHL*$^{flox/flox}$ mice; H. Saya and M.C. Simon for fruitful suggestions; T. Muraki, A. Kumakubo, and T. Hirose for essential support; and F. Arai, T. Naito, N. Tago, and A. Ono for FACS operation. K.T. was a research fellow of JSPS supported by the Global COE Programs for Human Metabolomic Systems Biology and for Stem Cell Medicine and also in part by a MEXT Grant-in-Aid for Young Scientists (B) and a Grant-in-Aid for Scientific Research on Priority Areas. A.H. and M.S. were supported in part by a MEXT Grant-in-Aid for Creative Scientific Research 17GS0419. M.S. supported FACS analysis as the Leader of ERATO, JST, Suematsu Gas Biology Project. T.S. was supported by a MEXT Grant-in-Aid for Specially Promoted Research.

Received: December 15, 2009
Revised: May 2, 2010
Accepted: June 9, 2010
Published: September 2, 2010

REFERENCES

Adelman, D.M., Maltepe, E., and Simon, M.C. (1999). Multilineage embryonic hematopoiesis requires hypoxic ARNT activity. Genes Dev. *13*, 2478–2483.

Arai, F., Hirao, A., Ohmura, M., Sato, H., Matsuoka, S., Takubo, K., Ito, K., Koh, G.Y., and Suda, T. (2004). Tie2/angiopoietin-1 signaling regulates hematopoietic stem cell quiescence in the bone marrow niche. Cell *118*, 149–161.

Cipolleschi, M.G., Dello Sbarba, P., and Olivotto, M. (1993). The role of hypoxia in the maintenance of hematopoietic stem cells. Blood *82*, 2031–2037.

Danet, G.H., Pan, Y., Luongo, J.L., Bonnet, D.A., and Simon, M.C. (2003). Expansion of human SCID-repopulating cells under hypoxic conditions. J. Clin. Invest. *112*, 126–135.

Haase, V.H., Glickman, J.N., Socolovsky, M., and Jaenisch, R. (2001). Vascular tumors in livers with targeted inactivation of the von Hippel-Lindau tumor suppressor. Proc. Natl. Acad. Sci. USA *98*, 1583–1588.

Hackney, J.A., and Moore, K.A. (2005). A functional genomics approach to hematopoietic stem cell regulation. Methods Mol. Med. *105*, 439–452.

Hermitte, F., Brunet de la Grange, P., Belloc, F., Praloran, V., and Ivanovic, Z. (2006). Very low O2 concentration (0.1%) favors G0 return of dividing CD34+ cells. Stem Cells *24*, 65–73.

Iwama, A., Oguro, H., Negishi, M., Kato, Y., Morita, Y., Tsukui, H., Ema, H., Kamijo, T., Katoh-Fukui, Y., Koseki, H., et al. (2004). Enhanced self-renewal of hematopoietic stem cells mediated by the polycomb gene product Bmi-1. Immunity *21*, 843–851.

Jang, Y.Y., and Sharkis, S.J. (2007). A low level of reactive oxygen species selects for primitive hematopoietic stem cells that may reside in the low-oxygenic niche. Blood *110*, 3056–3063.

Kiel, M.J., Yilmaz, O.H., Iwashita, T., Yilmaz, O.H., Terhorst, C., and Morrison, S.J. (2005). SLAM family receptors distinguish hematopoietic stem and progenitor cells and reveal endothelial niches for stem cells. Cell *121*, 1109–1121.

Kim, M., Cooper, D.D., Hayes, S.F., and Spangrude, G.J. (1998). Rhodamine-123 staining in hematopoietic stem cells of young mice indicates mitochondrial activation rather than dye efflux. Blood *91*, 4106–4117.

Kirito, K., Fox, N., Komatsu, N., and Kaushansky, K. (2005). Thrombopoietin enhances expression of vascular endothelial growth factor (VEGF) in primitive hematopoietic cells through induction of HIF-1alpha. Blood *105*, 4258–4263.

Kranc, K.R., Schepers, H., Rodrigues, N.P., Bamforth, S., Villadsen, E., Ferry, H., Bouriez-Jones, T., Sigvardsson, M., Bhattacharya, S., Jacobsen, S.E., et al. (2009). Cited2 is an essential regulator of adult hematopoietic stem cells. Cell Stem Cell *5*, 659–665.

Kubota, Y., Takubo, K., and Suda, T. (2008). Bone marrow long label-retaining cells reside in the sinusoidal hypoxic niche. Biochem. Biophys. Res. Commun. *366*, 335–339.

Kuhn, R., Schwenk, F., Aguet, M., and Rajewsky, K. (1995). Inducible gene targeting in mice. Science *269*, 1427–1429.

Levesque, J.P., Winkler, I.G., Hendy, J., Williams, B., Helwani, F., Barbier, V., Nowlan, B., and Nilsson, S.K. (2007). Hematopoietic progenitor cell mobilization results in hypoxia with increased hypoxia-inducible transcription factor-1 alpha and vascular endothelial growth factor A in bone marrow. Stem Cells *25*, 1954–1965.

Li, L., and Xie, T. (2005). Stem cell niche: Structure and function. Annu. Rev. Cell Dev. Biol. *21*, 605–631.

Liu, J., Cao, L., Chen, J., Song, S., Lee, I.H., Quijano, C., Liu, H., Keyvanfar, K., Chen, H., Cao, L.Y., et al. (2009). Bmi1 regulates mitochondrial function and the DNA damage response pathway. Nature *459*, 387–392.

Lo Celso, C., Fleming, H.E., Wu, J.W., Zhao, C.X., Miake-Lye, S., Fujisaki, J., Cote, D., Rowe, D.W., Lin, C.P., and Scadden, D.T. (2009). Live-animal tracking of individual haematopoietic stem/progenitor cells in their niche. Nature *457*, 92–96.

Miyamoto, K., Araki, K.Y., Naka, K., Arai, F., Takubo, K., Yamazaki, S., Matsuoka, S., Miyamoto, T., Ito, K., Ohmura, M., et al. (2007). Foxo3a is essential for maintenance of the hematopoietic stem cell pool. Cell Stem Cell *1*, 101–112.

Morrison, S.J., and Spradling, A.C. (2008). Stem cells and niches: Mechanisms that promote stem cell maintenance throughout life. Cell *132*, 598–611.

Naka, K., Muraguchi, T., Hoshii, T., and Hirao, A. (2008). Regulation of reactive oxygen species and genomic stability in hematopoietic stem cells. Antioxid. Redox Signal. *10*, 1883–1894.

Oguro, H., Yuan, J., Ichikawa, H., Ikawa, T., Yamazaki, S., Kawamoto, H., Nakauchi, H., and Iwama, A. (2010). Poised lineage specification in multipotential hematopoietic stem and progenitor cells by the polycomb protein Bmi1. Cell Stem Cell *6*, 279–286.

Osawa, M., Hanada, K., Hamada, H., and Nakauchi, H. (1996). Long-term lymphohematopoietic reconstitution by a single CD34-low/negative hematopoietic stem cell. Science *273*, 242–245.

Parmar, K., Mauch, P., Vergilio, J.A., Sackstein, R., and Down, J.D. (2007). Distribution of hematopoietic stem cells in the bone marrow according to regional hypoxia. Proc. Natl. Acad. Sci. USA *104*, 5431–5436.

Pedersen, M., Lofstedt, T., Sun, J., Holmquist-Mengelbier, L., Pahlman, S., and Ronnstrand, L. (2008). Stem cell factor induces HIF-1alpha at normoxia in hematopoietic cells. Biochem. Biophys. Res. Commun. *377*, 98–103.

Ryan, H.E., Lo, J., and Johnson, R.S. (1998). HIF-1 alpha is required for solid tumor formation and embryonic vascularization. EMBO J. *17*, 3005–3015.

Scadden, D.T. (2006). The stem-cell niche as an entity of action. Nature *441*, 1075–1079.

Semenza, G.L. (2007). Hypoxia-inducible factor 1 (HIF-1) pathway. Sci. STKE *2007*, cm8.

Simon, M.C., and Keith, B. (2008). The role of oxygen availability in embryonic development and stem cell function. Nat. Rev. Mol. Cell Biol. *9*, 285–296.

Sudo, K., Ema, H., Morita, Y., and Nakauchi, H. (2000). Age-associated characteristics of murine hematopoietic stem cells. J. Exp. Med. *192*, 1273–1280.

Sugiyama, T., Kohara, H., Noda, M., and Nagasawa, T. (2006). Maintenance of the hematopoietic stem cell pool by CXCL12-CXCR4 chemokine signaling in bone marrow stromal cell niches. Immunity *25*, 977–988.

Takubo, K., Ohmura, M., Azuma, M., Nagamatsu, G., Yamada, W., Arai, F., Hirao, A., and Suda, T. (2008). Stem cell defects in ATM-deficient undifferentiated spermatogonia through DNA damage-induced cell-cycle arrest. Cell Stem Cell *2*, 170–182.

Tanaka, T., Wiesener, M., Bernhardt, W., Eckardt, K.U., and Warnecke, C. (2009). The human HIF (hypoxia-inducible factor)-3alpha gene is a HIF-1 target gene and may modulate hypoxic gene induction. Biochem. J. *424*, 143–151.

Tipping, A.J., Pina, C., Castor, A., Hong, D., Rodrigues, N.P., Lazzari, L., May, G.E., Jacobsen, S.E., and Enver, T. (2009). High GATA-2 expression inhibits human hematopoietic stem and progenitor cell function by effects on cell cycle. Blood *113*, 2661–2672.

Tothova, Z., Kollipara, R., Huntly, B.J., Lee, B.H., Castrillon, D.H., Cullen, D.E., McDowell, E.P., Lazo-Kallanian, S., Williams, I.R., Sears, C., et al. (2007). FoxOs are critical mediators of hematopoietic stem cell resistance to physiologic oxidative stress. Cell *128*, 325–339.

Xie, Y., Yin, T., Wiegraebe, W., He, X.C., Miller, D., Stark, D., Perko, K., Alexander, R., Schwartz, J., Grindley, J.C., et al. (2009). Detection of functional haematopoietic stem cell niche using real-time imaging. Nature *457*, 97–101.

Yoshihara, H., Arai, F., Hosokawa, K., Hagiwara, T., Takubo, K., Nakamura, Y., Gomei, Y., Iwasaki, H., Matsuoka, S., Miyamoto, K., et al. (2007). Thrombopoietin/MPL signaling regulates hematopoietic stem cell quiescence and interaction with the osteoblastic niche. Cell Stem Cell *1*, 685–697.